Chemical Engineering Journal 435 (2022) 134883

Contents lists available at ScienceDirect

Chemical Engineering Journal

journal homepage: www.elsevier.com/locate/cej

Chemical looping reforming for syngas generation at real process conditions in packed bed reactors: An experimental demonstration

Panagiotis Alexandros Argyris [a], Christopher de Leeuwe [a], Syed Zaheer Abbas [a], Alvaro Amieiro [b], Stephen Poultson [b], David Wails [b], Vincenzo Spallina [a,*]

[a] Department of Chemical Engineering and Analytical Science, University of Manchester, Manchester M13 9PL, United Kingdom
[b] Johnson Matthey Technology Centre, Reading RG4 9NH, United Kingdom

ARTICLE INFO

Keywords:
Chemical looping
CO_2 capture
H_2 production
Packed bed reactor
High pressure

ABSTRACT

Chemical looping reforming (CLR) is a promising technology for syngas production combining autothermal operation with integrated CO_2 capture. At large scale, reformer outlet pressure during syngas production is an important factor for the overall plant's process efficiency and defines the energy requirements for downstream processing. Packed bed reactors are widely used and established in industry for high pressure operating conditions due to their robust and, compared to other reactor types, simpler engineering. In this paper, CLR in packed bed reactors (CLR-PB) is demonstrated under a pressure range of 1 – 5 bar in a lab scale reactor, using $NiO/CaAl_2O_4$ as the oxygen carrier (OC). Oxidation, reduction and dry reforming processes were examined in a wide range of temperature (400 – 900 °C), pressure (1 – 5 bar), flowrate (10 – 40 NLPM) and different inlet gas compositions, providing an important foreground for the optimal operating conditions for each process.

Furthermore, a full CLR-PB pseudo-continuous cycle has been successfully demonstrated for the first time in a lab reactor setup. During the full cycle operation, CH_4 conversion > 99% has been achieved, while the temperature and concentration profiles provided identical results for consecutive cycles verifying the continuity and the feasibility of the process. These results constitute the basis for the scale-up of the process, where heat losses would be minimized and the energy efficiency of the process would be significantly higher.

1. Introduction

The production of hydrogen (H_2) and other gas-to-liquid (GTL) products such as ammonia, methanol or Fischer-Tropsch fuels are of vital importance in the global chemical products market. The global demand for these products is mainly (60%) satisfied by the reforming of natural gas (NG) or oil and naphtha reforming [1]. However, in addition to having a high operation and capital costs, the conventional reforming techniques are also responsible for a large fraction of the chemical industry's CO_2 emissions [2]. NG reforming is conventionally carried out using either fired tubular reforming (FTR) or autothermal reforming (ATR). These methods differ on how the heat required for the endothermic reforming process is delivered to the system. In fired tubular reforming, the NG and either H_2O or CO_2 is fed through the tubes filled with catalyst while the outside of the tubes is immersed in a combustion furnace. In case of ATR, air or oxygen is added to the NG and H_2O in an adiabatic reactor [3] so that the heat for reforming is provided by the methane partial oxidation. Both these methodologies require actions to reduce greenhouse gases (GHGs) emissions in order to mitigate the environmental impact following the recommendations of Paris Agreement [4,5]. Different options have been demonstrated in the literature to capture the CO_2 produced during the reforming process including solvent absorption or through the use of membrane systems, but these options have very high capital and operating costs [6,7].

An alternative approach to produce syngas is by making use of chemical looping processes [8–10]. Chemical looping technologies present an interesting alternative for power and H_2 production combined with CO_2 capture while they present higher efficiency than conventional CO_2 capture technologies [11,12]. Chemical looping combustion (CLC) is based on two reactors, an air reactor (AR) and a fuel reactor (FR), where combustion is taking place in two stages by means of a metal oxygen carrier (OC) which is alternatively reduced (in the FR) and oxidised (in the AR) [13–16]. The main products from the reduction step (in the FR), are CO_2 and H_2O, where pure CO_2 can be easily separated by simple water condensation featuring the same advantages of oxy-combustion process. The heat stream generated from the oxidation (highly exothermic reaction) of the OC can be used as a thermal source

* Corresponding author.
E-mail address: vincenzo.spallina@manchester.ac.uk (V. Spallina).

https://doi.org/10.1016/j.cej.2022.134883
Received 9 November 2021; Received in revised form 20 January 2022; Accepted 21 January 2022
Available online 29 January 2022

Nomenclature

Abbreviations

AR	Air reactor
ATR	Autothermal reforming
CLC	Chemical looping combustion
CLR	Chemical looping reforming
CLR-PB	Chemical looping reforming in packed bed reactors
DMR	Dry methane reforming
FR	Fuel reactor
FTR	Fired Tubular Reforming
GTL	Gas to liquid
NLPM	Normal liter per minute
OC	Oxygen carrier
RWGS	Reverse water gas shift
SMR	Steam methane reforming
TC	Thermocouple
TRL	Technology readiness levels
WGS	Water gas shift

Symbols

$c_{p,g}$	gas specific heat capacity, J kg^{-1} K^{-1}
$c_{p,s}$	solid specific heat capacity, J kg^{-1} K^{-1}
$\Delta H_{R,ox}$	enthalpy of reaction for oxidation, J mol^{-1}
MW_{O_2}	O_2 molecular weight, kg mol^{-1}
$MW_{OC,act}$	Active OC molecular weight, kg mol^{-1}
T	Temperature, ^oC
u_s	Superficial gas velocity, m^3_g m^{-2}_r s^{-1}
ξ	O_2 to solid mole oxidation reaction ratio
$\omega_{gO_2,0}$	Initial O_2 mass fraction
$\omega_{OC,act}$	Active OC solid mass fraction

for power generation. Using the same principles as in the CLC, chemical looping technologies can be deployed in combination with reforming reactions. This is referred to as chemical looping reforming (CLR). In CLR, heat generated from the oxidation stage is used for the endothermic reactions of steam or dry reforming to produce syngas.

In terms of OCs, nickel has been widely used as an OC and a reforming catalyst. It is often supported on Al_2O_3, $CaAl_2O_4$, TiO_2 or ZrO_2 [17–19] to increase the mechanical and the chemical stabilities as well as to reduce the catalyst sintering. Most of the research on CLR has been carried under ambient pressure conditions [20], however, high pressure chemical looping shows several advantages from a techno-economic point of view and has been studied using different reactor configurations [21–23]. In case of syngas production, industrial applications are conceived at high pressure (20–26 bar [24]) to reduce the cost of compression, separation and the equipment footprint as in the case of large commercial ammonia, methanol or GTL processes. Among different configurations proposed [25–29], dynamically operated packed bed reactors have been proposed for chemical looping [30] and demonstrated up to TRL3/4 for CLC [31,32] and or in combination with calcium looping to simultaneously remove the CO_2 produced and increase the H_2 yield [33].

The CLR process in packed bed reactors (CLR-PB) consists of three reactor stages as shown in Fig. 1. Firstly, the bed is oxidized with air, producing heat from the exothermic reactions and releasing N_2 (O_2-depleted) as an outlet gas. The second step is to reduce the bed with off-gas fuel (a mixture of CO, H_2 and other small quantities light hydrocarbons), releasing CO_2 and H_2O while most of the heat is still in the bed. The last step is the reforming stage, using CH_4 and part of the recirculated CO_2 and H_2O from the reduction stage while simultaneously cooling down the reactor before starting a new oxidation cycle. In order to increase the CH_4 conversion, additional steam should be fed to the last stage [34]. Concerning the industrial application of CLR-PB, Spallina et al. [20] have been performed two techno-economic studies for the integration of CLR-PB to a hydrogen, methanol [35] and ammonia [36] plant, where over 99% CO_2 capture showing better economics compared to bechmark processes. At each stage of the above processes, the generation of low-grade fuels can be used to reduce the bed during the CLR process. Some of the most important CLR-PR units tested in the literature are presented in Table 1.

All the CLR-PB studies mentioned in Table 1 refer to atmospheric

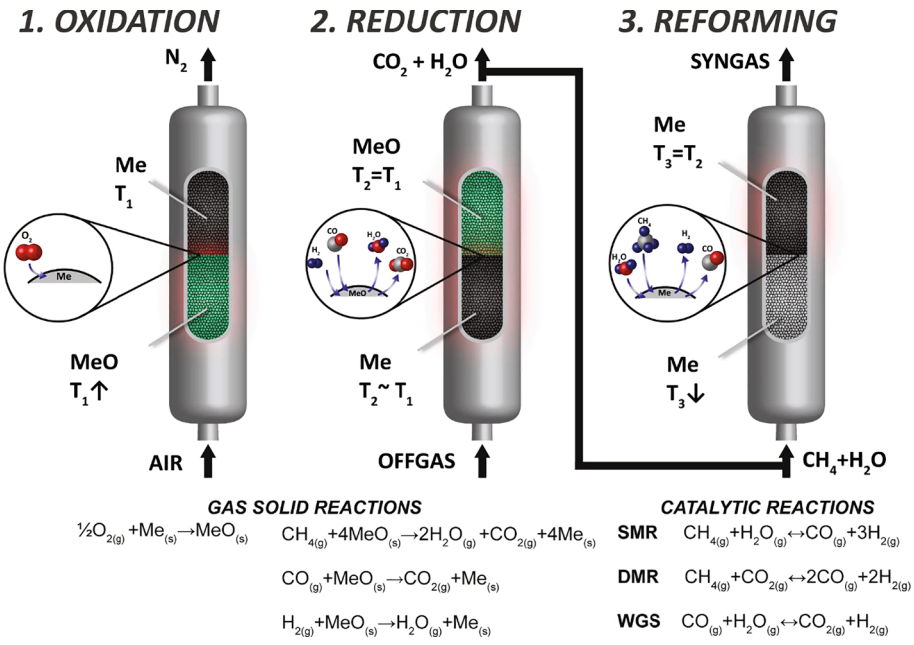

Fig. 1. Schematic of CLR-PB process steps.

Table 1
Summary of CLR applications in packed bed reactors.

Location	Reactor Size	Fuel	Oxygen Carrier	Reference
The University of Leeds, UK	ID:20.5 mmL:269 mm	Waste Cooking Oil (WCO)Pyrolysis OilAcetic acidEthanol/bio-oil aqueous fractionMixture	18 wt% NiO/Al_2O_3(i) 18 wt% NiO/α- Al_2O_3(ii) 25 wt% NiO/γ- Al_2O_3	[37,38][39] [40][41]
Eindhoven University of Technology (TU/e), The Netherlands	ID:30 mmL:1500 mm	$CH_4 + H_2$, CH_4	17–18.5 wt% NiO/$CaAl_2O_4$	[20]
University of Shanghai for Science and Technology, China	Bench scale	Ethanol	(i) 10.2 wt% NiO/ Al_2O_3(ii) 9.8 wt% NiO/ MMT(iii) 10.8 wt% NiO/Al-MCM-41(iv) 11.6 NiO/SBA-15	[42]
Dalian University of Technology, China	Bench scale	Glycerol	NiO/ Al_2O_3	[43]
Dalian University of Technology, China	Bench scale	Ethanol	(i) 10 wt% NiO/MMT(ii) 20 wt% NiO/MMT (iii) 30 wt% NiO/MMT	[44]
Instituto de Carboquímica (ICB-CSIC), Spain	ID:27 mmL:745 mm	$CH_4 + H_2$, H_2	(i) 21 wt% NiO/γ- Al_2O_3(ii) 18 wt% NiO/ α- Al_2O_3	[45]
Aristotle University of Thessaloniki,Greece	Bench scale	CH_4	(i)100 wt% NiO(ii-vi) 40 wt% NiO/ZrO_2/ TiO_2/ SiO_2/ Al_2O_3/$NiAl_2O_4$	[46]
Chalmers University of Technology, Sweden	Quartz reactor	CH_4	La_x Sr_{1-x} FeO_3-δ (x = 0.5, 0.8, 1)	[47]
Texas A and M University at Qatar and others	Bench scale	$CH_4 + H_2$, H_2	(i) 40 wt% NiO/ Al_2O_3(ii) 40 wt% NiO/ ZrO_2	[48]
Center for Research and Technology-Hellas (CERTH), Greece	Quartz reactor	CH_4	$La_{1-x}Sr_xM_yFe_{1-y}O_3$(M = Ni, Co, Cr, Cu)	[49]
State Key Laboratory of Complex Nonferrous Metal Resources Clean Utilization, Kunming University of Science and Technology, Yunnan, China	Quartz reactor	CH_4	Ce-Fe-Zr-O(40 wt%)/MgO	[50]

pressure conditions. Hamers et al. [31] have investigated CLC in packed bed reactors at elevated pressures (up to 7.5 bar). To the best of our knowledge, elevated pressure operation in CLR-PB units has not been investigated so far. In this paper, CLR stages (oxidation – reduction – dry reforming) are investigated in various operating conditions such as composition, initial bed temperature, flowrate and pressure. The experiments are conducted in a packed bed reactor with Ni/$CaAl_2O_4$ used as an OC. Moreover, a pseudo-continuous CLR-PB operation in a packed bed reactor is demonstrated for the first time in literature.

2. Experimental setup

The experiments have been conducted in the laboratory facility located at the University of Manchester. The overall experimental system is divided between two adjacent walk-in fume cupboards. Gases feeding arrangement and gas analysis equipment, mass spectrometer (Hiden QGA) and a CO analyser (Siemens), are placed in fume cupboard – 1 (FC-1) as shown in Fig. 2(a), while while the FC-2 contains the reactor setup along with the Carbolite® furnace controller as shown in Fig. 2(b). The gas feeding consists of central supply of H_2, Air, N_2, He as well as the gas cylinders of CO and CO_2, all capable of supplying a 5-bar pressure feed into the reactor system. The feed flowrates are controlled by Bronkhorst mass flow controllers and a Bronkhorst back-pressure regulator defines the pressure at the outlet of the reactor. Piping consists of quarter and half inch stainless steel welded and mounted pipes in solid surfaces. A schematic of the chemical looping packed bed reactor is shown in Fig. 3. The set up consists of a high temperature resistant stainless steel tube (253MA material manufactured by Array Industries B.V) with inner diameter and length of 35 mm and 1050 mm respectively. The reactor can be operated with the maximum temperature of 1000 °C and pressure of 20 bar. Inside the reactor, there is a thermowell of 1050 mm length and 6.3 mm diameter having 10 K-type thermocouples (TC) mounted on it to measure the temperature along the length of the bed. Each TC is 75 mm apart from each other. The temperature of the reactor is regulated by a vertical split furnace (up to 1000 °C). To mitigate the heat losses, the pipework before and after the reactor were insulated using ceramic wool. The reactor was filled with an inert material (Al_2O_3) at the bottom and top of the reactor to ensure that the OC

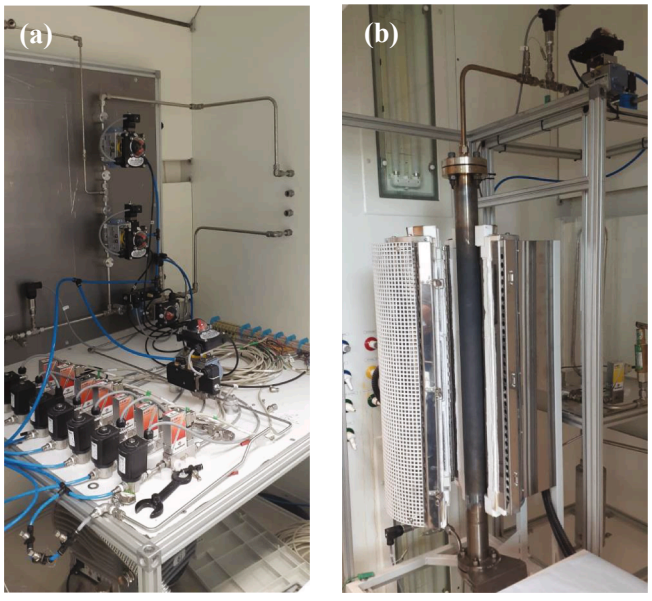

Fig. 2. (a) Gas feeding system placed in FC-1 (b) Packed bed reactor system placed in FC-2 at University of Manchester.

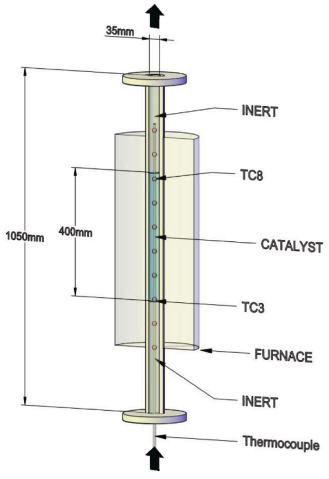

Fig. 3. Schematic of cross section of the CLR-PB unit.

material is held in the middle of the reactor where the temperatures is most tightly controlled. This also allowed for some preheating of the inlet gas to the reaction temperature. The middle of the reactor was packed with 440 g of a Ni based OC supported on $CaAl_2O_4$ manufactured by Johnson Matthey. This material was crushed to particle size of 1–1.4 mm and the loose packed density was found to be 1127 kg m^{-3}. The total length of reactive material inside the bed was 400 mm. Thermocouple 3 (TC3) is located at the beginning of the reactive bed ($z = 0$ mm) while the last thermocouple inside the bed is TC8 ($z = 375$ mm). The reactor exhaust is air cooled to remove the water content before the dry gas composition is determined using a combination of a mass spectrometer and a CO analyser. A P&ID of the whole system is presented in Fig. 4. The valves and mass flow controllers are controlled by a custom-build HMI which also records temperatures from the thermocouples and the pressure from pressure indicators. A second HMI unit was used for the operation of the mass spectrometer and the CO analyser.

3. Results and discussion

The OC is tested under various operating conditions of pressure (1 – 5 bar), temperature (400 – 900 °C), flowrates (10 – 40 NLPM) and compositions of feed gases. In the following section, the oxidation step/process is discussed followed by the reduction and dry reforming. The detailed results of each stage are reported in this section.

3.1. Oxidation stage

The operating conditions used for the oxidation stage are listed in Table 2.

3.1.1. Effect of initial solid temperature and pressure

The initial bed temperature has a strong effect on the oxidation process. The profiles of outlet molar composition of O_2 for various initial bed temperatures (400 – 650 °C) and pressures (1 – 5 bar) are presented in Fig. 5. Due to the heat losses and cooling effect of the feeding gases, the temperature is not uniform across the bed, with the first part (first 100 mm) being 50–100 °C cooler than the initial bed temperature. For the oxidation at 400 °C, the breakthrough of O_2 is very quick, almost immediate (<20 s) at lower pressure conditions. The low reactivity of the Ni-based material at 400 °C along with the heat losses prevents the

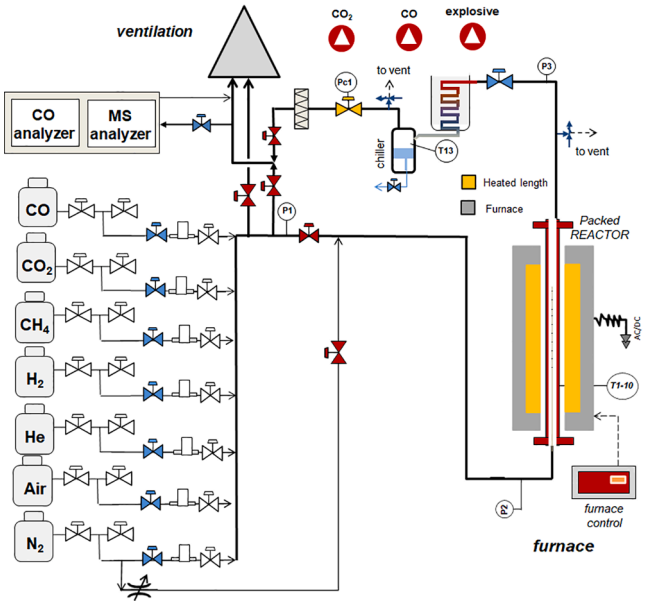

Fig. 4. P&ID diagram of the CLR-PB setup.

Table 2
The operating conditions used for the oxidation stage.

Flowrates (NLPM)	Pressure (bar)	Initial bed temperature (°C)	O_2 % (molar)
10	1–5	400–650	5 – 20
20	1–5	600	10
40	1–5	600	10

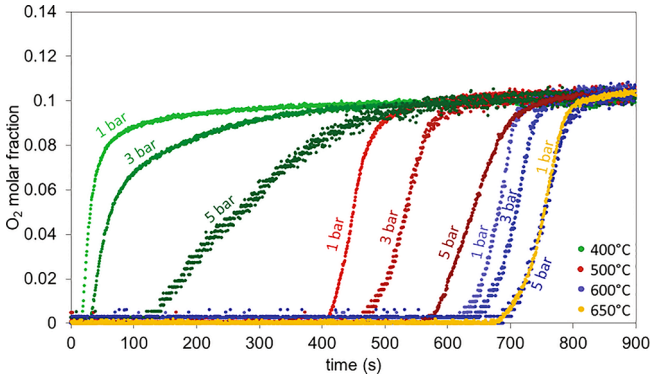

Fig. 5. O_2 breakthrough profile during oxidation for 10% O_2 and 10 NLPM of feed (50% Air, 10% He and 40% N_2) under various operating conditions of temperature (400 – 650) and pressure (1 – 5 bar).

O_2 to react and increase the temperature (as expected in case of exothermic oxidation) to the final reaction temperature, thus reducing the overall OC conversion to 10% of the maximum conversion achieved for 10 NLPM flowrate and 10% O_2. By increasing the initial solid temperature to 500 °C, O_2 breakthrough time is significantly increased, about 415 s for 1 bar, and the solid conversion reaches almost 60%. For the oxidation at 600 °C, O_2 breakthrough time increased to 625 s for 1 bar while for 650 °C, time increased up to 680 s which was the highest observed for the examined cases. In this work, temperature higher than 650 °C has not been tested to avoid an excessive overheating of the reactor (to preserve the OC from sintering and the reactor from reaching a temperature > 1000 °C).

Fig. 5 also shows the O_2 breakthrough times for the various pressure conditions (1 – 5 bar). Increasing pressure results in later O_2 breakthrough as observed earlier for all the temperature conditions. This is mostly due to two main effects: 1) the gas velocity inside the bed decreases with an increase in pressure, thus increasing the residence time and 2) the effect of pressure in the kinetics. This is particularly pronounced for the cases at 400 °C, where the kinetic limitations are higher. This result is also verified by the temperature profiles along the bed and the rise in temperature with time due to the exothermic oxidation

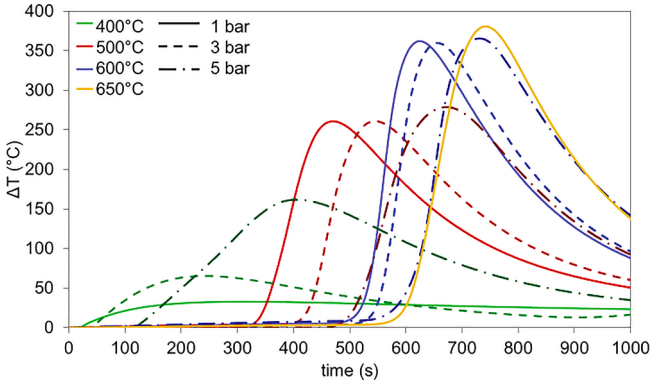

Fig. 6. The change in temperature profile at TC-7 (z = 0.3 m) as a function of time during the oxidation process for 10% O_2 and 10NLPM.

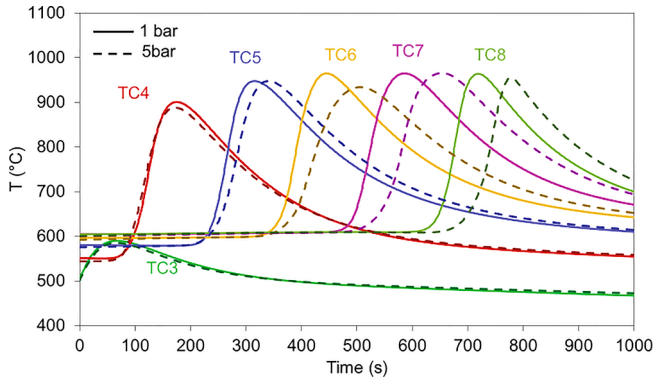

Fig. 7. Thermocouples' recording temperature during oxidation for 1 bar (solid lines) and 5 bar (dashed lines), 10% O_2 in feed, 600 °C initial bed temperature and 10 NLPM feed flowrate.

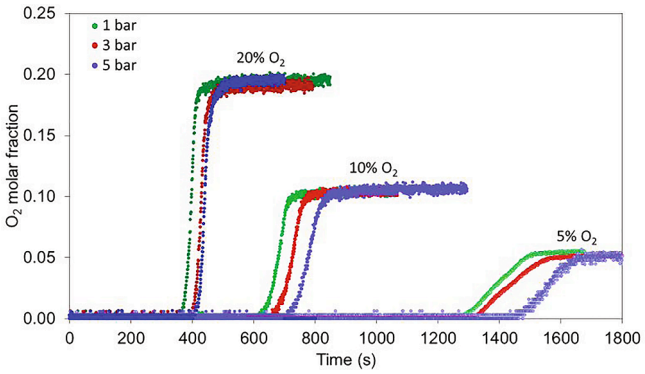

Fig. 8. Comparison of O_2 breakthrough times for various O_2 concentration (5 – 20 % O_2) and pressure (1 – 5 bar) conditions at initial bed temperature of 600 °C and feed flowrate of 10 NLPM.

reaction as shown in Fig. 6.

The increase in temperature at the reaction front is well detected all over the reactor. At 400 °C and 1 bar, temperature rise (defined in Equation (1) [51]) is 32 °C maximum, indicating that solid conversion is very low while it increases to 161 °C at 5 bar, demonstrating the big effect pressure has on the solid conversion especially at this temperature range. At higher initial temperature (same for 600 °C and 650 °C), the ΔT increases up to 378 °C while the difference in time to record the peak is smoothed showing a lower (but still remarkable) effect of the pressure.

With respect to maximum ΔT, the presence of heat losses and the thermal inertia of the thermowell located inside the bed reduces by 310 °C the maximum expected value for the 650 °C bed temperature case where maximum conversion for the given conditions has been achieved. This effect has been widely discussed in previous work from Gallucci et al. [32].

The comparison of temperature profiles along the axial direction of the reactor for 1 and 5 bar conditions at 600 °C initial bed temperature is illustrated in Fig. 7. In the first part of the bed (TC3 and TC4), the profiles look very similar, but due to better solid conversion at higher pressures, the difference between the two cases is amplified across the bed.

The effect of pressure on solid conversion has been studied by Hamers et al. [52] where they showed that higher pressure leads to slower conversion of the solid and therefore slower kinetics. This comes in agreement with the sharper breakthrough lines produced in lower pressures in Fig. 5 but does not justify the higher conversion leading to higher ΔT produced in Fig. 6. The OC in their study has been tested against oxidation at 800 °C leading to full solid conversion for all the pressure scenarios, which is far from the temperature range examined here (400 – 650 °C). Additional kinetic studies are required to demonstrate the effect of pressure for the selected catalyst at temperatures as low as 400 °C especially in terms of solid conversion. In addition, the behaviour of the catalyst might differ in the context of a full bed oxidation than a kinetic study due to different flow conditions.

3.1.2. *Effect of oxygen concentration*

In this section the effect of O_2 concentration (5%, 10% and 20%) on the O_2 breakthrough is discussed. The 20% case refers to an industrial application where air will be used as oxidant with a 10% helium used here as a gas tracer. Fig. 8 shows that O_2 breakthrough time decreases with the increase in O_2 concentration. Moreover, the breakthrough curve of O_2 becomes steeper as the contraction of O_2 increases due to faster oxidation kinetics [53].

As discussed earlier, it can also be seen in Fig. 9 that with the increase in pressure the O_2 breakthrough time also increases. The breakthrough times are not exactly halved for each O_2 concentration case as the solid conversion is different for each case and due to the uncertainty

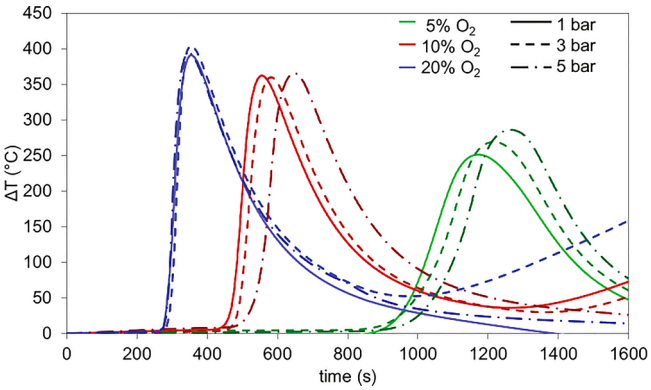

Fig. 9. the rise in temperature rise as recorded at TC6 (z = 0.225 m) for different O_2 concentrations and pressures at 600 °C initial bed temperature and 10NLPM total flowrate.

associated with the flowrate regulators.

The maximum temperature rise in the bed is affected by the O_2 content in the feed gases. In Fig. 9, the temperature profile for thermocouple 6 (TC6) is presented. For lower O_2 content in the feed, the maximum temperature rise should be higher and more dispersed across the reactor as indicated from Equation (1). The higher temperature increase displayed for higher O_2 concentration is attributed to the shorter cycles and therefore reduced cooling by heat losses effect. The rise in temperature at TC6 is 220 °C, 350 °C and 370 °C for the cases where O_2 concentration in the feed is 5%, 10 and 20% respectively. In Fig. 10, the maximum temperature rise for all the cases with a 10 NLPM flowrate is

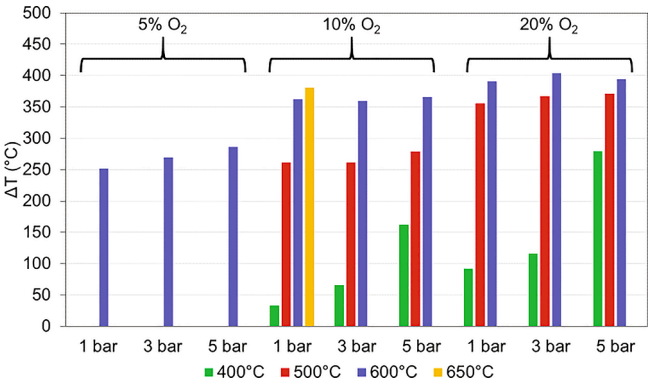

Fig. 10. Temperature rise for all the examined oxidation cases at 10 NLPM total flowrate.

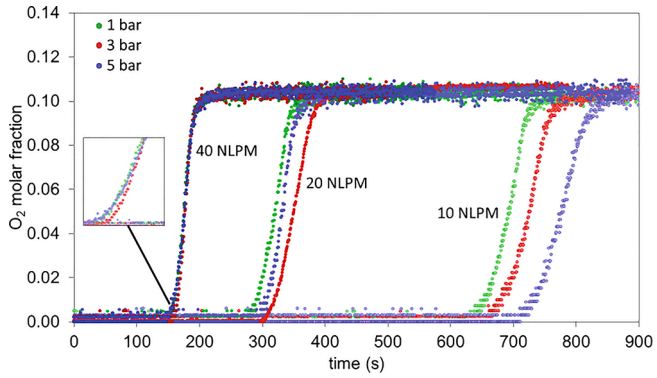

Fig. 11. O_2 breakthrough times for different flowrates at initial bed temperature of 600 °C and 10% O_2 concentration in the feed.

presented. Increasing the O_2 concentration increases maximum temperature significantly from 251 °C at 5% to 390 °C at 20% for 1 bar which emphasizes the important effect of the heat losses in the system.

$$\Delta T_{MAX} = \frac{\left(-\Delta H_{R,ox}\right)}{\frac{c_{p,s}MW_{OC,act}}{\omega_{OC,act}\xi} - \frac{c_{p,g}MW_{O_2}}{\omega_{gO_2,0}}} \quad (1)$$

3.1.3. Effect of gas velocity and residence time

The effect of feed flowrate, and thus the superficial gas velocity, has been tested for 3 different flowrate conditions of 10, 20 and 40 NLPM, which for the 1 bar and 600 °C cases refer to superficial velocities approximately at 0.1, 0.5 and 1 m s^{-1} respectively, with the latter case representing the typical industrial conditions. In Fig. 11, the O_2 breakthrough times indicate that with the increase of flowrate the effect of pressure is becoming less evident and at the 40 NLPM can be considered negligible. The high flowrate effect comes in agreement with the results of Hamers et al. [31], where they used a high flowrate oxidation stream and no difference has been observed in the breakthrough times with varying pressure.

In terms of temperature, the feed flowrate of 40 NLPM causes the highest rise in temperature as shown in Fig. 12. This behaviour can be explained by the larger oxidation times at lower flowrates leading to larger exposure to heat losses. The deviation for the 20 NLPM and 3 bar case, is a result of minor carbon deposition from previous experiments even though no significant CO_2 or CO were detected. Carbon presence during oxidation results in later breakthrough times and higher temperature rise due to carbon burning which comes in agreement to this result. In terms of pressure drop, even for the high flowrate cases it was found negligible.

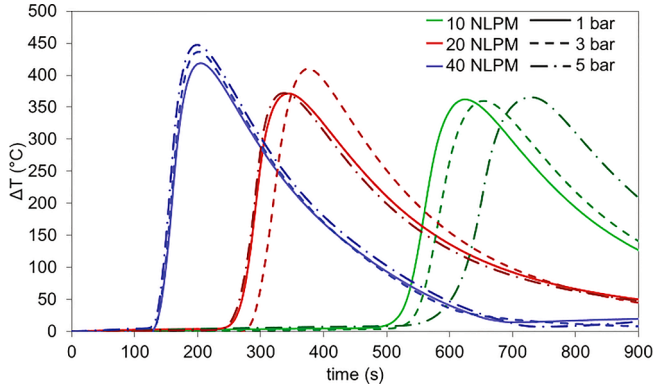

Fig. 12. Oxidation temperature rise as recorded by TC7 (z = 0.3 m) for different O2 concentrations and pressures at 600 °C initial bed temperature.

Table 3
Experimental operating conditions during reduction stage.

Conditions	H_2	Syngas	CH_4-rich
Flowrate (NLPM)	10	10	12
Initial bed temperature (°C)	600–900	600 – 900	600 – 900
Pressure (bar)	1–5	1–5	1–5
Gas composition (vol %)			
He	10	10	41.7
N_2	70	–	–
CO_2	–	70	50
CO		10	
H_2	20	10	–
CH_4	–	–	8.3

3.2. Reduction stage

NiO reduction experiments have been conducted with H_2, syngas and CH_4 as reduction gases. The conditions used for these experiments are presented in Table 3. For CH_4 reduction, a 6:1 CO_2 to CH_4 ratio has been used to avoid the carbon deposition. This ratio is also representative of an industrial application of a CLR-PB process, where the reduction agent is the off-gas from the PSA unit mixed with additional natural gas to close the combustion equilibrium of the CLR process. Previous studies on industrial applications of CLR-PB have demonstrated that the CO_2:CH_4 ratio is usually in the range of 6:1 – 7:1 depending on the process with smaller amounts of CO and H_2 existing on the stream as well [35,36,54].

3.2.1. Reduction with H_2

The effect of initial bed temperature on the breakthrough of H_2 molar fraction (dry basis) at the outlet of the reactor during the reduction stage is shown in Fig. 13 where with the increase in bed temperature, the breakthrough times also increase. For the initial bed temperature of 600 °C and 20% H_2 in the feed, H_2 concentration doesn't reach 20% at the outlet of the reactor after the reduction indicating a very slow reaction rate happening over time. As the initial solid temperature increases, the breakthrough slope becomes sharper and the breakthrough occurs later (from 450 s at 600 °C to 870 s at 900 °C) as more solid is reduced.

3.2.2. Reduction with syngas

During the reduction of Ni based OC with syngas, CO_2 is also used in the feeding mixture to simulate a realistic industrial reduction application (e.g. PSA off-gas [20]). Due to the presence of CO_2 in syngas, catalytic reactions (DMR and WGS) also take place which shift the composition of the products after the material is completely reduced and the bed behaves as a catalytic reactor. In Fig. 14, the relationship between CO and H_2 breakthrough times and initial bed temperature is shown. As expected, a higher temperature increases the amount of solid due to bed activation resulting in a longer cycle time. Once the bed is completely reduced, CO, H_2 and CO_2 are present in the products due to

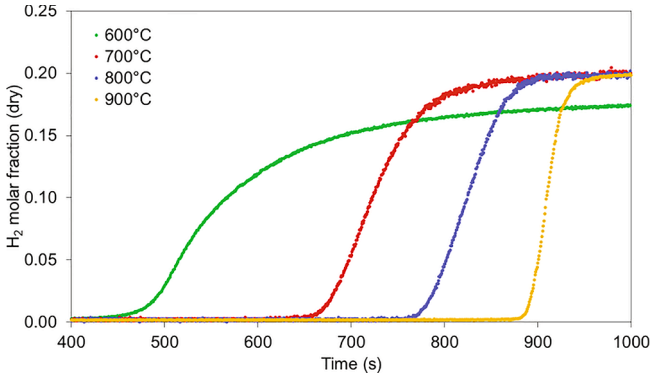

Fig. 13. H_2 breakthrough for different initial bed temperatures at 3 bar.

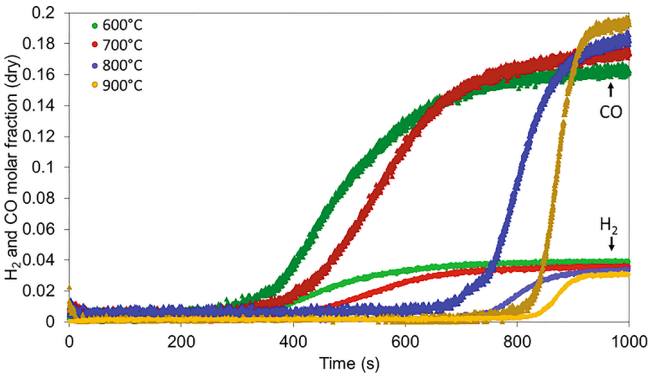

Fig. 14. CO and H_2 breakthrough times for reduction with syngas at different initial bed temperatures and 3 bar conditions.

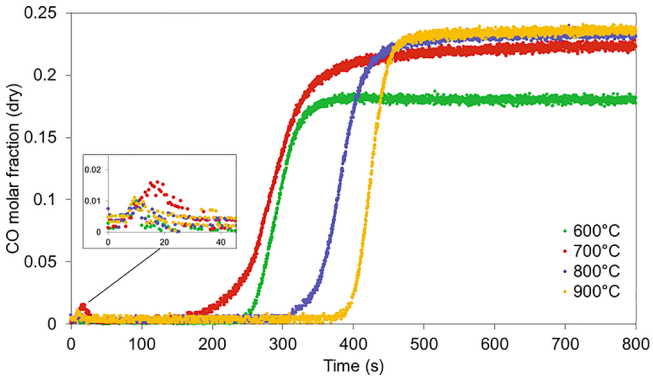

Fig. 16. CO breakthrough times for reduction with CH_4 at different initial bed temperature and 1 bar conditions.

the reverse WGS (RWGS) reaction that also changes the mole fractions. CO breakthrough occurs faster than the breakthrough of H_2 for all temperature, pressure, flowrates and composition cases, and results are in agreement with the published work of Medrano et al. [53].

3.2.3. *Reduction with CH_4-rich gas*

The breakthrough curves during the reduction with CH_4–rich gas are shown in Fig. 15. It can be seen that CH_4 is converting the Ni based OC, producing CO_2 and H_2O apart from a minor CH_4 slippage (2%) at the beginning of the reduction for 8 s. CH_4 is reacting with CO_2 (DMR and RWGS) under the operating conditions of 900 °C and 1 bar pressure and once the solid is converted syngas is detected at the outlet of the reactor.

The effect of temperature on the CO breakthrough during the reduction with CH_4-gas is presented in Fig. 16. At the part of the bed where the OC is in reduced form, DMR and RWGS are also taking place. The temperature trend shows later breakthrough curves with increasing temperature apart from the 700 °C case. The reason of an earlier breakthrough at 700 °C is dictated by the fact that the thermodynamic equilibrium at 600 °C shows a high H_2 production compared to the other temperatures under consideration due to the competing effect of dry reforming and RWGS (both favoured at high temperature). Since less solid conversion is achieved with CO than with H_2, the breakthrough is faster at 700 °C. With an increase in temperature, the faster kinetics for NiO reduction delay the breakthrough up to 400 s (at 900 °C) with a full NiO conversion.

According to Le Chatelier's principle, the increase of pressure would not be beneficial for the dry reforming reaction, so maximum CH_4 conversion will be achieved at lower pressures. In our experiments, 1 bar is the lowest pressure used, so maximum CH_4 conversion is expected for the 1 bar case. In Fig. 17, CH_4 is fully converted for all the cases except for the 600 °C where CH_4 slippage is 1% on dry basis at the outlet of the reactor. For all the temperatures, there is a breakthrough of CH_4 during

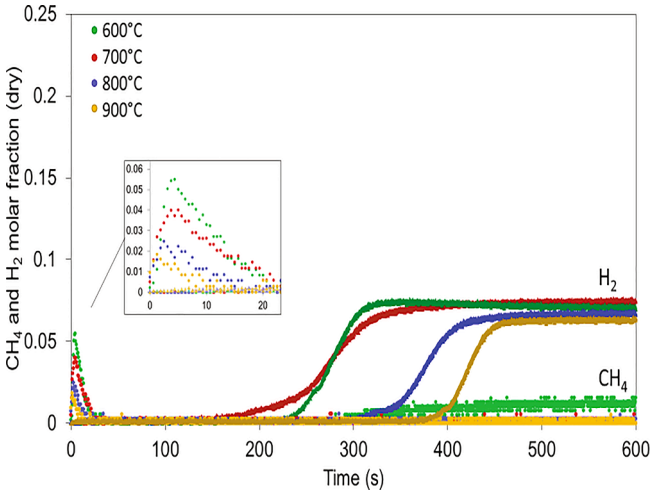

Fig. 17. CH_4 and H_2 breakthrough curves for reduction with CH_4 at different initial bed temperatures and 1 bar pressure.

the first 20 s of reduction. This is an effect encountered in all the examined cases at all pressure conditions, and the early CH_4 and CO breakthrough amounts are presented in Fig. 18. These amounts are connected also to the previous oxidation where solid has not been 100 % converted so there is some Ni available. For 1 bar, the amount is higher at lower temperatures, while at higher pressures, the amount seems to

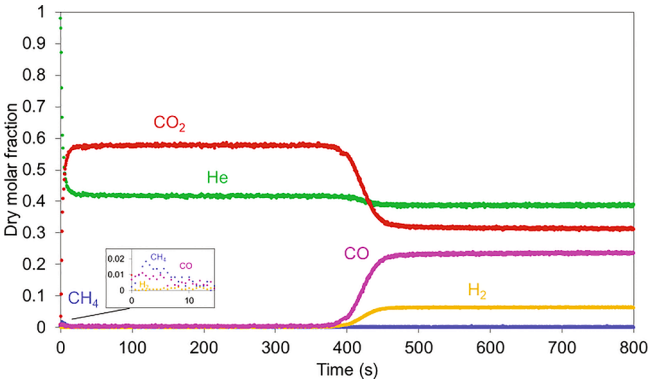

Fig. 15. Breakthrough curves during reduction with CH_4 at 900 °C and 1 bar.

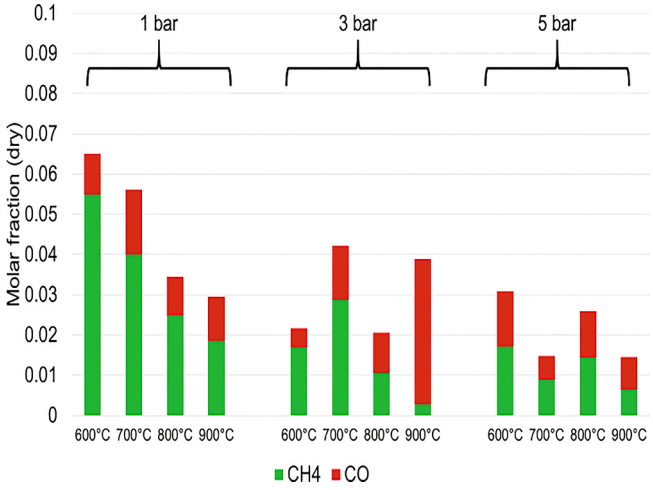

Fig. 18. Early CH_4 and CO breakthrough during NiO reduction with CH_4.

be smaller but no proper conclusion can be derived given the combination of gas–solid and catalytic reactions. As confirmed also in Medrano et al. [53], NiO reduction with CH_4 does not occur at lower temperatures (500 – 700 °C) and this could partially explain the presence of unconverted gases at the beginning. Previous studies on NiO-supported on alumina have shown that both CH_4 and other hydrocarbons are converted at temperatures close to 550 °C [55] and 600 °C [56], while at high temperature (>900 °C) NiO (supported on $NiAl_2O_4$, $MgAl_2O_4$, TiO_2 and ZrO_2) reacts with CH_4 as well [57]. This could be explained by the interaction with the support material ($CaAl_2O_4$) that inhibits CH_4 to properly reduce NiO.

While H_2 and syngas reduction are slightly exothermic reactions (ΔH^o_{298K} = -2.125 kJ/mol$_{H2}$ ΔH^o_{298K} = -43.26 kJ/mol$_{CO}$ respectively) keeping the bed temperature constant, the reduction with CH_4 is mostly endothermic (ΔH^o_{298K} = 156.5 kJ/mol$_{CH4}$). As shown in Fig. 19, the bed responds differently with the increase in temperature and pressure. At the beginning of the bed (where TC3 is located, z = 0 mm), the temperature drops due to the endothermic reactions (mainly DMR). While considering a different position of the OC inside the reactor (at 75 mm where TC4 is located), the bed initially shows an increase in temperature due to the exothermic reactions with CO and H_2 consumed via OC reduction in the previous part of the bed. As the initial bed temperature increases, the temperature drop is larger but more limited in the first part of the bed, mostly because of the increase in both the reforming reaction extent and the heat losses. Increasing pressure results in smaller temperature drop due to shifting in the equilibrium of the dry reforming reaction but is almost marginal given the pressure interval studied (1–5 bar). The second half of the bed maintains the set temperature for all the cases, slowly presenting small peaks of temperature with increasing initial bed temperature as previously discussed for the case of syngas.

3.3. Dry reforming stage

Dry reforming has been tested as heat removal stage and syngas production to complete the overall process cycle and deliver the valuable products for downstream synthesis and conditioning. The operating conditions used for the dry reforming are listed in Table 4.

3.3.1. Effect of temperature and pressure

The effect of temperature and pressure on dry reforming is presented in Fig. 20. The endothermic nature of the reaction is evident in all the cases. As the initial bed temperature increases, the temperature drop also increases and it becomes limited to the first part of the bed (TC3-TC5). Increasing pressure results in lower temperature drop with time as the dry reforming reaction becomes less active.

3.3.2. Effect of CO_2 to CH_4 ratio (CO_2/CH_4)

The CO to H_2 ratio (CO/H_2) produced during the dry reforming stage for the various cases listed in Table 4 is presented in Fig. 21. As expected, increasing temperature and CO_2/CH_4 ratio produce more CO at the outlet of the reactor. As temperature increases from 700 to 900 °C at CO_2/CH_4 of 3.0, CO/H_2 increases from 1.54 to 1.73. Similarly for the CO_2/CH_4 of 7.0, with the increase in temperature from 700 to 900 °C, CO/H_2 increases from 3.17 to 3.92. Moreover, CO/H_2 increases with pressure as predicted from Le Chatelier's principle.

All the cases with CO_2/CH_4 equal to 3.0 produced carbon deposition with increased carbon formation at lower temperature and increasing pressure due to the Boudouard reaction. For CO_2/CH_4 of 4.0, only the cases with initial solid temperature of 900 °C did not show carbon deposition, minor amount was found at 800 °C and significant amount was observed for the 700 °C in particular at 5 bar.

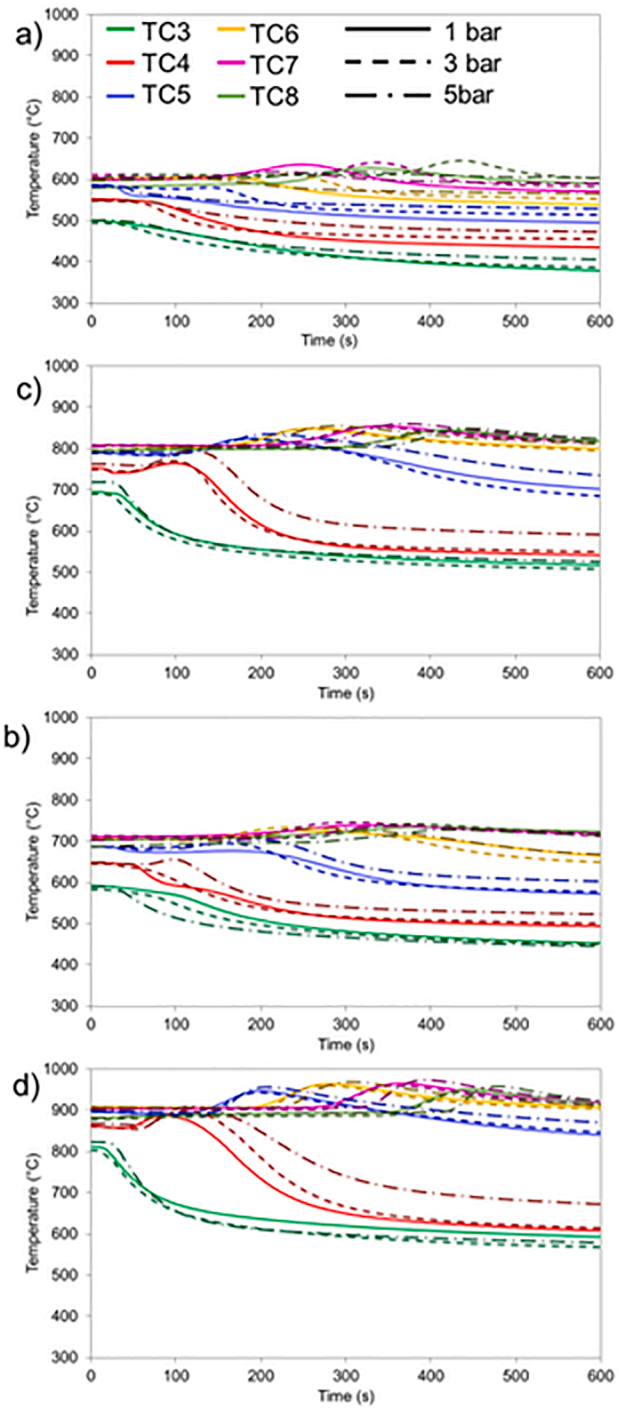

Fig. 19. Bed thermocouples recording temperatures for CH_4 reduction for a) 600 °C b) 700 °C c) 800 °C and d) 900 °C initial bed temperature.

Table 4
Experimental operating conditions during the dry reforming.

CO_2/CH_4	3:1	4:1	5:1	6:1	7:1
Flowrate (NLPM)	10	11	12	12	12
Initial bed temperature (°C)	700–900	700 – 900	700 – 900	700 – 900	700 – 900
Pressure (bar)	1 – 5	1 – 5	1 – 5	1 – 5	1 – 5
Gas composition (vol %)					
He	60.0	54.5	50.0	41.7	33.3
CO_2	30.0	36.4	41.7	50.0	58.3
CH_4	10.0	9.1	8.3	8.3	8.3

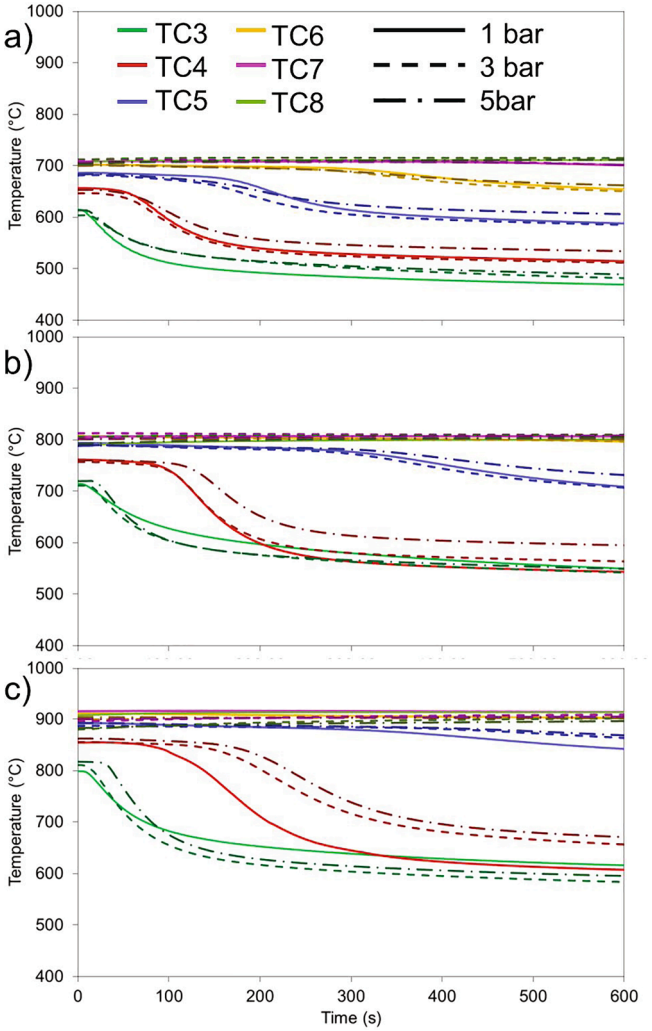

Fig. 20. Thermocouples' recording temperature for a)700 °C b) 800 °C c) 900 °C initial bed temperature with a CO_2:CH_4 6:1 ratio.

From Fig. 22, the experimental results match well with the thermodynamic equilibrium values obtained from ASPEN GIBBS reactor under the operating of various temperature (700 – 900 °C) and CO_2/CH_4 of 6.0.

3.4. Complete CLR cycle/process

A complete CLR-PB sequence of operation has been performed for the first time in an experimental packed bed reactor at this scale with

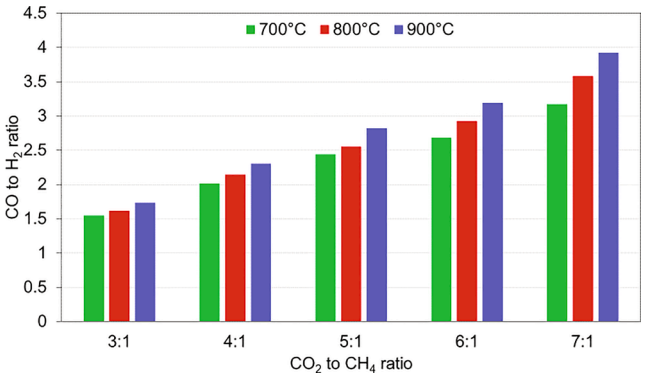

Fig. 21. CO/H_2 produced for the examined dry reforming cases under various operating conditions of temperature and 1 bar pressure.

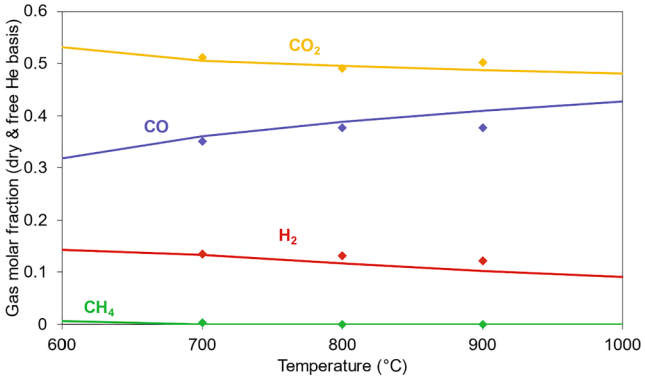

Fig. 22. Experimental dry gas composition for CO_2:CH_4 6:1 and 1 bar pressure compared to thermodynamic equilibrium given by ASPEN Gibbs reactor. Dots are the experimental results and solid lines are the equilibrium values.

repeated cycles and controlled heat losses. Oxidation, reduction and reforming flowrates and compositions have been set to produce similar reactor cycle times and the various parameters are presented in Table 5. The furnace temperature was set at 600 °C to avoid excessive heat losses associated with the lab scale experiments while preserving the nature of the experiment where a pseudo-adiabatic condition was replicated. At industrial scale, by using an internal diameter > 2 m and a refractory layer as additional insulation [31], the heat losses become negligible, therefore the minimum temperature of the reactor would be the one at the end of the reforming (approximately 600 °C). Moreover the temperature of the feeding gases in the industrial scale is in the range of 500 – 600 °C as opposed to the initial ambient temperatures used in the conducted experiments, therefore the preheating of gases via the furnace becomes imminent. By keeping the furnace at 600 °C, we were able to replicate a close operating condition of industrial scale reactor, thus demonstrating that the heat for the endothermic reforming can be provided by the heat generated via chemical looping redox reactions directly at the solid surface. As the effect of pressure was found negligible in the previous analysis, the experiments were conducted at 1 bar. Initially, air (mixed with 10% He) was fed to the bed for 180 s with the main products being N_2 and He as shown in Fig. 23. The oxidation was stopped at 180 s before O_2 breakthrough. At 180 s, N_2 is purged through the bed to remove any remaining O_2 in the reactor before the start of reduction stage. During reduction, CO_2 and H_2O are produced, H_2O is not shown (dry composition) and N_2 is used as an inert carrier gas. CH_4-rich gas with CO_2 (CO_2:CH_4 ratio equal to 6:1) is used for both the

Table 5
Inlet operating conditions for the CLR complete cycle (furnace temperature at 600 °C and pressure at 1 bar).

Inlet conditions	Oxidation	Purge	Reduction	Reforming	Purge	Purge
Flow Rate (NLPM)	10	7	14	14	13	7
Feed time (s)	180	60	190	180	40	150
Molar Fraction %						
N_2	71.1	100.0	50.0		53.8	100.0
O_2	18.9	–	–		–	–
He	10.0	–	–		–	–
CO_2	–	–	42.9		46.2	–
CH_4	–	–	7.1		–	–

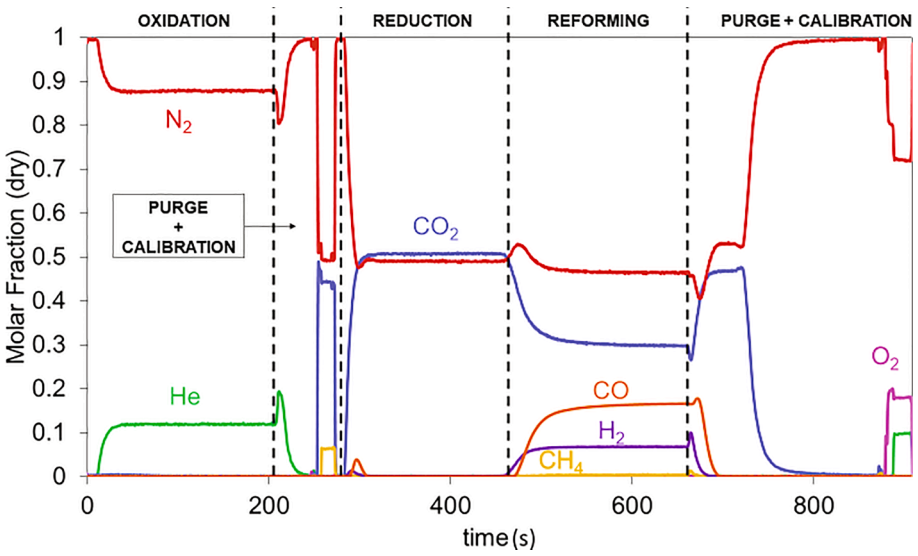

Fig. 23. Outlet molar fractions (dry) during complete CLR cycle.

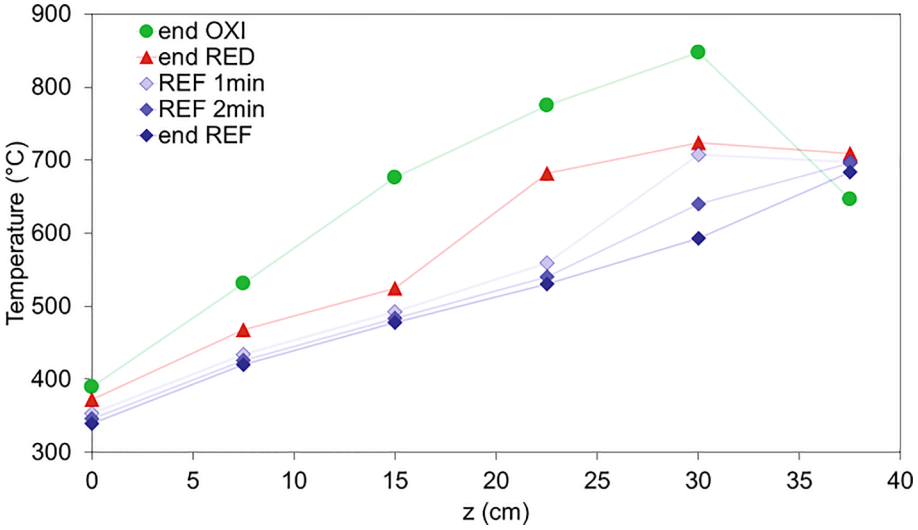

Fig. 24. Axial bed temperatures for the end of reduction (green circles), end of reduction (red triangles) and the evolution of reforming (blue diamonds) during the CLR continuous operation. (For interpretation of the references to colour in this figure legend, the reader is referred to the web version of this article.)

reduction and the reforming stage. Catalytic reactions (DMR and WGS) take place in the part of the bed that is still in reduced form. As expected from the previous analysis, a small quantity of syngas is detected at the very beginning, while fuel conversion into CO_2 and H_2O is complete during the reduction. At 190 s of reduction, the bed has reacted completely and starts to behave as catalytic reactor with reforming occurring, to produce syngas. CH_4 breakthrough is below 0.1%. After 180 s of reforming, the system is purged to completely remove any fuel remaining in the bed and proceed to the next oxidation stage. Three complete cycles have been performed presenting good repeatability even though this system does not use an automated valve operation (detailed results of consecutive cycles are shown in Figures A1 and A2 in supplementary material).

The experiment has been designed so that most of the heat will be

still present at the beginning of reforming as shown in Fig. 24. The highest temperature in the bed is encountered at the end of oxidation at bed length of 300 mm, equal to 850 °C. During the reduction with CH_4, heat is partially removed from the bed. Some heat is also lost to the surroundings with the gases leaving the bed at approximately 700 °C. During the dry reforming, most of the heat is removed leaving only the last part of the bed at 700 °C which is the part of the bed where CH_4 is already converted and no reforming is occurring as discussed in section 3.3.

The demonstration of the continuous CLR-PB process provides the foreground for the industrial scale-up of the process. The process is repeated with the same results, confirming its feasibility even at a lab reactor scale, with manual valve switching and significant heat losses. The material has been tested against over 480 h of CLR operation without any noticeable drop in performance, making it a strong candidate for the OC choice. Industrial scale reactors for the CLR-PB process are expected to approximate adiabatic behaviour due to their larger diameter (0.5 – 3.5 m) as demonstrated in previous studies [37]. In the smaller diameter cases, minimization of heat losses can be achieved via proper insulation of the system. The system parameters can also be optimized (catalyst active material, dimensions of the reactor, cycle times) to achieve the best possible efficiency for the desired product demands. An industrial scale system would require at least 3 reactors (oxidation – reduction – reforming), supply of steam for mixing during reforming and purges, proper insulation to minimize heat losses and automatic valve operation timed for the required reactor stages. A complete operation strategy for the industrial scale operation has been demonstrated in previous studies [20,36].

4. Conclusion

In this study, the CLR-PB using a $NiO/CaAl_2O_4$ OC has been studied in a range of operating conditions including pressures up to 5 bar. Pressure was found to be an important factor in oxidation in low velocity operation ($u_s \approx 0.1$ m s^{-1}) where higher pressures produced better solid conversion, while it showed no difference under industrial conditions ($u_s \approx 1$ m s^{-1}). The solid conversion during oxidation increased with increase in bed temperature with 400 °C being the lowest with almost instant O_2 breakthrough and 650 °C the highest with a temperature increase of 380 °C. In all reduction experiments, the trend showed an increase in conversion and faster kinetics with the increase in temperature. CO breakthrough appeared earlier than H_2 in syngas reduction indicating that H_2 is a better reduction agent. The CH_4 was reformed to syngas by the active Ni catalytic sites in the bed which further reduced it. Dry reforming presented the expected conversion results with CO_2/CH_4 ratios below 5 causing carbon deposition.

The pseudo-continuous CLR-PB operation has been successfully demonstrated showing good repeatability in the results for several cycles and a $>$ 99% CH_4 conversion, proving the CLR-PB concept to be feasible for the first time experimentally. The successful demonstration of the process in a lab-scale reactor provides a very strong foreground for the applicability and the scale-up of the process.

Declaration of Competing Interest

The authors declare that they have no known competing financial interests or personal relationships that could have appeared to influence the work reported in this paper.

Acknowledgements

The authors acknowledge the EPSRC project (BREINSTORM - EP/S030654/1) and the UKCCSRC (UKRI funded project) for providing funding and support to development of this study. The authors would like to take this opportunity to recognize the important contribution to this paper, and many other areas of hydrogen and reforming technologies, of their late and much missed friend and colleague David Wails who prematurely died during the preparation of this manuscript.

Appendix A. Supplementary data

Supplementary data to this article can be found online at https://doi.org/10.1016/j.cej.2022.134883.

References

[1] N. Muradov, T. Vezirolu, From hydrocarbon to hydrogen-carbon to hydrogen economy, Int. J. Hydrogen Energy. 30 (3) (2005) 225–237, https://doi.org/10.1016/j.ijhydene.2004.03.033.
[2] IEA, Technology Roadmap: Energy and GHG Reductions in the Chemical Industry via Catalytic Processes, 2015.
[3] A.M.W. P. Haussinger, R. Lohmuller, 2. Production Wiley (Ed.), Ullman's Encyclopedia of Industrial Chemistry (2012), pp. 249-298, in: Hydrogen, 2012.
[4] United Nations, Paris Agreement on Climate Change (2015) 1.
[5] Committee on Climate Change, UK climate change following the Paris Agreement, 2016.
[6] G. Collodi, G. Azzaro, N. Ferrari, S. Santos, Techno-economic Evaluation of Deploying CCS in SMR Based Merchant H2 Production with NG as Feedstock and Fuel, Energy Procedia, Elsevier 114 (2017) 2690–2712, https://doi.org/10.1016/j.egypro.2017.03.1533.
[7] J.C. Abanades, B. Arias, A. Lyngfelt, T. Mattisson, D.E. Wiley, H. Li, M.T. Ho, E. Mangano, S. Brandani, Emerging CO2 capture systems, Int. J. Greenh. Gas Control. 40 (2015) 126–166, https://doi.org/10.1016/j.ijggc.2015.04.018.
[8] J. Adanez, A. Abad, F. Garcia-Labiano, P. Gayan, L.F. de Diego, Progress in chemical-looping combustion and reforming technologies, Prog. Energy Combust. Sci. 38 (2) (2012) 215–282, https://doi.org/10.1016/j.pecs.2011.09.001.
[9] M. Luo, Y. Yi, S. Wang, Z. Wang, M. Du, J. Pan, Q. Wang, Review of hydrogen production using chemical-looping technology, Renew. Sustain. Energy Rev. 81 (2018) 3186–3214, https://doi.org/10.1016/j.rser.2017.07.007.
[10] D. Li, R. Xu, X. Li, Z. Li, X. Zhu, K. Li, Chemical Looping Conversion of Gaseous and Liquid Fuels for Chemical Production: A Review, Chemical Looping Conversion of Gaseous and Liquid Fuels for Chemical Production: A Review 34 (5) (2020) 5381–5413, https://doi.org/10.1021/acs.energyfuels.0c01006.
[11] V. Spallina, M.C. Romano, P. Chiesa, F. Gallucci, M. van Sint Annaland, G. Lozza, Integration of coal gasification and packed bed CLC for high efficiency and near-zero emission power generation, Int. J. Greenh. Gas Control. 27 (2014) 28–41, https://doi.org/10.1016/j.ijggc.2014.04.029.
[12] B. Erlach, M. Schmidt, G. Tsatsaronis, Comparison of carbon capture IGCC with pre-combustion decarbonisation and with chemical-looping combustion, Energy. 36 (6) (2011) 3804–3815, https://doi.org/10.1016/j.energy.2010.08.038.
[13] M. Rydén, A. Lyngfelt, T. Mattisson, Chemical-looping combustion and chemical-looping reforming in a circulating fluidized-bed reactor using Ni-based oxygen carriers, Energy and Fuels. 22 (4) (2008) 2585–2597, https://doi.org/10.1021/ef800065m.
[14] A. Abad, J. Adánez, A. Cuadrat, F. García-Labiano, P. Gayán, L.F. de Diego, Kinetics of redox reactions of ilmenite for chemical-looping combustion, Chem. Eng. Sci. 66 (4) (2011) 689–702, https://doi.org/10.1016/j.ces.2010.11.010.
[15] S. Noorman, M. Van Sint Annaland, H. Kuipers, Packed bed reactor technology for chemical-looping combustion, Ind. Eng. Chem. Res. 46 (2007) 4212–4220, https://doi.org/10.1021/ie061178i.
[16] I. Iliuta, R. Tahoces, G.S. Patience, S. Rifflart, F. Luck, Chemical-looping combustion process: Kinetics and mathematical modeling, AIChE J. 56 (2010) 1063–1079, https://doi.org/10.1002/AIC.11967.
[17] A. Nandy, C. Loha, S. Gu, P. Sarkar, M.K. Karmakar, P.K. Chatterjee, Present status and overview of Chemical Looping Combustion technology, Renew. Sustain. Energy Rev. 59 (2016) 597–619, https://doi.org/10.1016/j.rser.2016.01.003.
[18] L.F. de Diego, M. Ortiz, F. García-Labiano, J. Adánez, A. Abad, P. Gayán, Hydrogen production by chemical-looping reforming in a circulating fluidized bed reactor using Ni-based oxygen carriers, J. Power Sources. 192 (1) (2009) 27–34, https://doi.org/10.1016/j.jpowsour.2008.11.038.
[19] M. Ortiz, L.F. de Diego, A. Abad, F. García-Labiano, P. Gayán, J. Adánez, Hydrogen production by auto-thermal chemical-looping reforming in a pressurized fluidized bed reactor using Ni-based oxygen carriers, Int. J. Hydrogen Energy. 35 (1) (2010) 151–160, https://doi.org/10.1016/j.ijhydene.2009.10.068.
[20] V. Spallina, B. Marinello, F. Gallucci, M.C. Romano, M. Van Sint Annaland, Chemical looping reforming in packed-bed reactors: Modelling, experimental validation and large-scale reactor design, Fuel Process. Technol. 156 (2017) 156–170. https://doi.org/10.1016/j.fuproc.2016.10.014.
[21] M. Osman, M.N. Khan, A. Zaabout, S. Cloete, S. Amini, Review of pressurized chemical looping processes for power generation and chemical production with integrated CO2 capture, Fuel Process. Technol. 214 (2021) 106684, https://doi.org/10.1016/j.fuproc.2020.106684.
[22] F. Kong, J. Swift, Q. Zhang, L.-S. Fan, A. Tong, Biogas to H2 conversion with CO2 capture using chemical looping technology: Process simulation and comparison to conventional reforming processes, Fuel. 279 (2020) 118479, https://doi.org/10.1016/j.fuel.2020.118479.
[23] C. Chen, G.M. Bollas, Optimal design of combined cycle power plants with fixed-bed chemical-looping combustion reactors, AIChE J. 65 (7) (2019), https://doi.org/10.1002/aic.16516.

[24] R.B. Gupta, Hydrogen fuel: production, transport, and storage, Crc Press, 2008.
[25] T.L. Hsieh, D. Xu, Y. Zhang, S. Nadgouda, D. Wang, C. Chung, Y. Pottimurphy, M. Guo, Y.Y. Chen, M. Xu, P. He, L.S. Fan, A. Tong, 250 kWth high pressure pilot demonstration of the syngas chemical looping system for high purity H2 production with CO2 capture, Appl. Energy. 230 (2018) 1660–1672, https://doi.org/10.1016/j.apenergy.2018.09.104.
[26] S.A. Wassie, J.A. Medrano, A. Zaabout, S. Cloete, J. Melendez, D.A.P. Tanaka, S. Amini, M. van Sint Annaland, F. Gallucci, Hydrogen production with integrated CO2 capture in a membrane assisted gas switching reforming reactor: Proof-of-Concept, Int. J. Hydrogen Energy. 43 (12) (2018) 6177–6190, https://doi.org/10.1016/j.ijhydene.2018.02.040.
[27] C. Park, T.-L. Hsieh, Y. Pottimurthy, V. Shah, D. Xu, Y.-Y. Chen, L.-S. Fan, A. Tong, Design and Operations of a 15 kWth Subpilot Unit for the Methane-to-Syngas Chemical Looping Process with CO2 Utilization, Ind. Eng. Chem. Res. 59 (15) (2020) 6886–6899, https://doi.org/10.1021/acs.iecr.9b05577.
[28] A. Bischi, Ø. Langørgen, J.-X. Morin, J. Bakken, M. Ghorbaniyan, M. Bysveen, O. Bolland, Performance analysis of the cold flow model of a second generation chemical looping combustion reactor system, Energy Procedia. 4 (2011) 449–456, https://doi.org/10.1016/j.egypro.2011.01.074.
[29] R. Xiao, L. Chen, C. Saha, S. Zhang, S. Bhattacharya, Pressurized chemical-looping combustion of coal using an iron ore as oxygen carrier in a pilot-scale unit, Int. J. Greenh. Gas Control. 10 (2012) 363–373.
[30] S. Noorman, M.V.S. Annaland, H. Kuipers, Packed Bed Reactor Technology for Chemical-Looping Combustion, Ind. Eng. Chem. Res. 46 (2007) 4212–4220, https://doi.org/10.1021/ie061178i.
[31] H.P. Hamers, F. Gallucci, G. Williams, M. Van Sint Annaland, Experimental demonstration of CLC and the pressure effect in packed bed reactors using NiO/CaAl2O4 as oxygen carrier, Fuel. 159 (2015) 828–836. https://doi.org/10.1016/j.fuel.2015.07.034.
[32] F. Gallucci, H.P. Hamers, M. van Zanten, M. van Sint Annaland, Experimental demonstration of chemical-looping combustion of syngas in packed bed reactors with ilmenite, Chemical Engineering Journal 274 (2015) 156–168.
[33] J.R. Fernandez, J.C. Abanades, R. Murillo, Modeling of sorption enhanced steam methane reforming in an adiabatic fixed bed reactor, Chem. Eng. Sci. 84 (2012) 1–11, https://doi.org/10.1016/j.ces.2012.07.039.
[34] V. Spallina, F. Gallucci, M. van Sint Annaland, Chemical Looping Processes Using Packed Bed Reactors, in: Handb. Chem. Looping Technol., Wiley-VCH Verlag GmbH & Co. KGaA, 2018: pp. 61–92. https://doi.org/10.1002/9783527809332.ch3.
[35] V. Spallina, G. Motamedi, F. Gallucci, M. van Sint Annaland, Techno-economic assessment of an integrated high pressure chemical-looping process with packed-bed reactors in large scale hydrogen and methanol production, Int. J. Greenh. Gas Control. 88 (2019) 71–84. https://doi.org/10.1016/j.ijggc.2019.05.026.
[36] R.J. Lee Pereira, P.A. Argyris, V. Spallina, A comparative study on clean ammonia production using chemical looping based technology, Appl. Energy. 280 (2020) 115874, https://doi.org/10.1016/j.apenergy.2020.115874.
[37] P. Pimenidou, G. Rickett, V. Dupont, M.V. Twigg, High purity H2 by sorption-enhanced chemical looping reforming of waste cooking oil in a packed bed reactor, Bioresour. Technol. 101 (23) (2010) 9279–9286, https://doi.org/10.1016/j.biortech.2010.06.079.
[38] P. Pimenidou, G. Rickett, V. Dupont, M.V. Twigg, Chemical looping reforming of waste cooking oil in packed bed reactor, Bioresour. Technol. 101 (16) (2010) 6389–6397, https://doi.org/10.1016/j.biortech.2010.03.053.
[39] A. Lea-Langton, R.M. Zin, V. Dupont, M.V. Twigg, Biomass pyrolysis oils for hydrogen production using chemical looping reforming, Int. J. Hydrogen Energy 37 (2) (2012) 2037–2043, https://doi.org/10.1016/j.ijhydene.2011.05.083.
[40] F. Cheng, V. Dupont, Nickel catalyst auto-reduction during steam reforming of bio-oil model compound acetic acid, Int. J. Hydrogen Energy. 38 (35) (2013) 15160–15172, https://doi.org/10.1016/j.ijhydene.2013.09.111.
[41] R. Md Zin, A.B. Ross, J.M. Jones, V. Dupont, Hydrogen from ethanol reforming with aqueous fraction of pine pyrolysis oil with and without chemical looping, Bioresour. Technol. 176 (2015) 257–266, https://doi.org/10.1016/j.biortech.2014.11.034.
[42] B. Dou, H. Zhang, G. Cui, Z. Wang, B.o. Jiang, K. Wang, H. Chen, Y. Xu, Hydrogen production and reduction of Ni-based oxygen carriers during chemical looping steam reforming of ethanol in a fixed-bed reactor, Int. J. Hydrogen Energy. 42 (42) (2017) 26217–26230, https://doi.org/10.1016/j.ijhydene.2017.08.208.
[43] B. Jiang, B. Dou, Y. Song, C. Zhang, B. Du, H. Chen, C. Wang, Y. Xu, Hydrogen production from chemical looping steam reforming of glycerol by Ni-based oxygen carrier in a fixed-bed reactor, Chem. Eng. J. 280 (2015) 459–467, https://doi.org/10.1016/j.cej.2015.05.120.
[44] B. Jiang, B. Dou, K. Wang, C. Zhang, Y. Song, H. Chen, Y. Xu, Hydrogen production by chemical looping steam reforming of ethanol using NiO/montmorillonite oxygen carriers in a fixed-bed reactor, Chem. Eng. J. 298 (2016) 96–106, https://doi.org/10.1016/j.cej.2016.04.027.
[45] M. Ortiz, L.F. de Diego, A. Abad, F. García-Labiano, P. Gayán, J. Adánez, Catalytic activity of ni-based oxygen-carriers for steam methane reforming in chemical-looping processes, Energy and Fuels. 26 (2) (2012) 791–800, https://doi.org/10.1021/ef2013612.
[46] A. Antzara, E. Heracleous, L. Silvester, D.B. Bukur, A.A. Lemonidou, Activity study of NiO-based oxygen carriers in chemical looping steam methane reforming, Catal. Today. 272 (2016) 32–41, https://doi.org/10.1016/j.cattod.2015.10.027.
[47] M. Rydén, A. Lyngfelt, T. Mattisson, D.e. Chen, A. Holmen, E. Bjørgum, Novel oxygen-carrier materials for chemical-looping combustion and chemical-looping reforming; LaxSr1-xFeyCo1-yO3-δ perovskites and mixed-metal oxides of NiO, Fe2O3 and Mn3O4, Int. J. Greenh. Gas Control. 2 (1) (2008) 21–36, https://doi.org/10.1016/S1750-5836(07)00107-7.
[48] L. Silvester, A. Antzara, G. Boskovic, E. Heracleous, A.A. Lemonidou, D.B. Bukur, NiO supported on Al2O3 and ZrO2 oxygen carriers for chemical looping steam methane reforming, Int. J. Hydrogen Energy. 40 (24) (2015) 7490–7501, https://doi.org/10.1016/j.ijhydene.2014.12.130.
[49] L. Nalbandian, A. Evdou, V. Zaspalis, La1-xSrxMyFe1-yO 3-δ perovskites as oxygen-carrier materials for chemical-looping reforming, Int. J. Hydrogen Energy. 36 (11) (2011) 6657–6670, https://doi.org/10.1016/j.ijhydene.2011.02.146.
[50] Y. Long, K. Li, Z. Gu, X. Zhu, Y. Wei, C. Lu, S. Lin, K. Yang, X. Cheng, D. Tian, F. He, H. Wang, Ce-Fe-Zr-O/MgO coated monolithic oxygen carriers for chemical looping reforming of methane to co-produce syngas and H2, Ce-Fe-Zr-O/MgO coated monolithic oxygen carriers for chemical looping reforming of methane to co-produce syngas and H 388 (2020) 124190, https://doi.org/10.1016/j.cej.2020.124190.
[51] S. Noorman, F. Gallucci, M. van Sint Annaland, J.A.M. Kuipers, A theoretical investigation of CLC in packed beds. Part 2: Reactor model, Chem. Eng. J. 167 (1) (2011) 369–376, https://doi.org/10.1016/j.cej.2011.01.012.
[52] H.P. Hamers, F. Gallucci, G. Williams, P.D. Cobden, M. Van Sint Annaland, Reactivity of oxygen carriers for chemical-looping combustion in packed bed reactors under pressurized conditions, Energy and Fuels. 29 (2015) 2656–2663. https://doi.org/10.1021/ef5027899.
[53] J.A. Medrano, H.P. Hamers, G. Williams, M. van Sint Annaland, F. Gallucci, NiO/CaAl2O4 as active oxygen carrier for low temperature chemical looping applications, Appl. Energy. 158 (2015) 86–96, https://doi.org/10.1016/j.apenergy.2015.08.078.
[54] P.A. Argyris, A. Wright, O. Taheri Qazvini, V. Spallina, Dynamic behaviour of integrated chemical looping process with pressure swing adsorption in small scale on-site H2 and pure CO2 production, Chem. Eng. J. 428 (2022) 132606.
[55] F. Cheng, V. Dupont, M.V. Twigg, Direct reduction of nickel catalyst with model bio-compounds, Appl. Catal. B Environ. 200 (2017) 121–132, https://doi.org/10.1016/J.APCATB.2016.06.044.
[56] V. Dupont, A.B. Ross, E. Knight, I. Hanley, M.V. Twigg, Production of hydrogen by unmixed steam reforming of methane, Chem. Eng. Sci. 63 (11) (2008) 2966–2979.
[57] T. Mattisson, M. Johansson, A. Lyngfelt, The use of NiO as an oxygen carrier in chemical-looping combustion, Fuel. 85 (5-6) (2006) 736–747.